Evolutionary design of a full-envelope full-authority flight control system for an unstable high-performance aircraft

G Avanzini and E A Minisci

Proceedings of the Institution of Mechanical Engineers, Part G: Journal of Aerospace Engineering 2011 225: 1065
originally published online 13 August 2011
DOI: 10.1177/0954410011414469

Evolutionary design of a full-envelope full-authority flight control system for an unstable high-performance aircraft

G Avanzini[1]* and **E A Minisci**[2]
[1]Faculty of Industrial Engineering, Università del Salento, Brindisi, Italy
[2]School of Engineering, University of Glasgow, Glasgow, UK

The manuscript was received on 29 October 2010 and was accepted after revision for publication on 1 June 2011.

DOI: 10.1177/0954410011414469

Abstract: The use of an evolutionary algorithm in the framework of H_∞ control theory is being considered as a means for synthesizing controller gains that minimize a weighted combination of the infinite norm of the sensitivity function (for disturbance attenuation requirements) and complementary sensitivity function (for robust stability requirements) at the same time. The case study deals with a complete full-authority longitudinal control system for an unstable high-performance jet aircraft featuring (i) a stability and control augmentation system and (ii) autopilot functions (speed and altitude hold). Constraints on closed-loop response are enforced, that representing typical requirements on airplane handling qualities, that makes the control law synthesis process more demanding.

Gain scheduling is required, in order to obtain satisfactory performance over the whole flight envelope, so that the synthesis is performed at different reference trim conditions, for several values of the dynamic pressure, used as the scheduling parameter. Nonetheless, the dynamic behaviour of the aircraft may exhibit significant variations when flying at different altitudes, even for the same value of the dynamic pressure, so that a trade-off is required between different feasible controllers synthesized at different altitudes for a given equivalent airspeed. A multi-objective search is thus considered for the determination of the best suited solution to be introduced in the scheduling of the control law. The obtained results are then tested on a longitudinal non-linear model of the aircraft.

Keywords: aircraft control system, robust control, multi-objective optimization

1 INTRODUCTION

In this article, a control synthesis technique in the framework of H_∞ control theory is proposed, based on the application of a modern multi-objective evolutionary optimization algorithm (MOEA) to the associated minimization problem. The objective is to derive a control system design tool that can successfully handle the complex scenario considered, where a complete full-authority longitudinal control system for a modern unstable high-performance jet aircraft is being designed, featuring (i) a stability and control augmentation system (SCAS) and (ii) autopilot functions (speed and altitude hold). Rather than simply demonstrating the capabilities of the optimization method, the objective of the research is more focused on the engineering aspects of the application of this innovative control synthesis approach to a challenging problem. Significant variations in the response of the system to control inputs are expected in the presence of control surface position and rate

*Corresponding author: Faculty of Industrial Engineering, Università del Salento, Cittadella della Ricerca, S.S. km. 7+300, 72100, Brindisi, Italy.
email: giulio.avanzini@unisalento.it

saturation, while enforcing demanding closed-loop performance constraints, representative of typical requirements on aircraft handling qualities.

In the past two decades, multiple redundant, full authority, fail/safe operational, fly-by-wire control systems have been brought to a very mature state. As a result, many aircraft, from earlier designs such as the F-16, F-18, and Tornado, through the more recent Mirage 2000, European Fighter Aircraft, Rafale, and advanced demonstrators such as X-29 and X-31, are highly augmented, actively controlled vehicles with marginal or even negative static stability without augmentation, for reasons related to improved performances, weight/cost reduction, and/or low observability [**1**].

Highly augmented and/or super-augmented aircraft require the synthesis of a control system that artificially provides the required level of stability for satisfactory handling qualities, enhancing pilot capability by properly tailoring aircraft response to manoeuvre state [**2**]. At the same time, modern high-performance jet aircraft are characterized by an extended flight envelope in order to allow the pilot to reach unprecedented manoeuvring capabilities at high angles of attack [**3**]. Such a result can be achieved only if the control system maintains adequate performance in the presence of considerable variations of aircraft response characteristics, compensating for inherent aerodynamic instabilities while providing adequate control power in the presence of control surface position and rate saturation limits, external disturbances, and model uncertainties.

The flight control system is often completed by auto-pilot functions, such as Mach, altitude, and heading hold, which allows for reducing pilot workload [**2**]. In this respect, a nested architecture is often adopted in the definition of the control system, where the inner loop provides high-gain stability and control augmentation for fast, short-period variables (attitude and angular velocity), while the outer auto-pilot loop takes care of low-bandwidth control tasks for slower trajectory variables (e.g. velocity and climb angle). This structure is often employed also in the framework of fully autonomous unmanned aerial vehicles (UAVs), where the problem of autonomously performing complex mission tasks outside of direct communication coverage from the ground station requires the development of high-level auto-pilot functions (such as autonomous landing [**4**]), nested around a full-authority stability augmentation system [**5**].

A (set of) robust controller(s) that provides adequate closed-loop performance in the presence of external disturbance and model uncertainties of known 'size' can be derived in the framework of H_∞ control theory [**6**]. H_∞ control systems have been studied for more than 20 years in the framework of aerospace applications, although these studies had limited impact on industrial practice, where more conventional approaches to control law synthesis are favoured. Nonetheless, H_∞ flight control systems have been flown in the past, with considerable success, on both manned [**7**, **8**] and unmanned vehicles [**9**].

H_∞ control requires that the controller is synthesized by minimizing the infinite norm of the system, determined as the maximum singular value $\bar{\sigma}$ of the transfer function matrix $\boldsymbol{G}(s)$ for a multi-input/multi-output (MIMO) system. In more physically meaningful terms, $\bar{\sigma}$ represents the maximum gain for a (disturbance) signal in the expected frequency range: the system is robust to the worst expected disturbance if $\bar{\sigma}$ is less than 1, in which case all the disturbances will be attenuated by the closed-loop system. The cost of robustness is a certain degree of 'conservativeness' of the controller, which may reduce closed-loop performance. For this reason, the requirement for robust stability may be accompanied by requirements in the time domain (such as raise time, overshoot, and settling time), that can be enforced as inequality constraints to the optimization problem in order to pursue a minimum acceptable level of performance.

In aircraft applications, these constraints can be easily derived from requirements on handling qualities, such as those reported in reference [**10**]. At the same time, the requirement for disturbance attenuation is limited to a given frequency range, where disturbances are expected to significantly affect closed-loop behaviour, so that weighting functions are used in order to properly tailor the requirement on $\bar{\sigma}$. Physical features of aircraft response may induce the presence of peaks in the frequency response that simply cannot be attenuated. A typical example is represented by the short- and long-term responses to elevator and throttle inputs of trajectory variables that are crucial for autopilot tasks.

The synthesis of the controller in the framework of H_∞ control theory is usually carried out by means of linear matrix inequalities (LMI) [**11**]. When a conventional approach based on the solution of LMI's is adopted for the design of an aircraft control system, handling quality requirements are enforced by properly tailoring the weights used during the control law design-phase and then checking the response of the closed-loop system *a posteriori*. This trial-and-error approach may prove to be difficult, especially when

control power is barely sufficient for the required control task. On the other hand, as underlined in reference [**12**], a control system design problem can be quite naturally formulated in terms of a constrained optimization problem, but the number of unknowns, non-linearities, and the presence of competing objectives make the resulting numerical solution extremely hard to obtain. The inherent difficulties of the problem can be tackled by means of an approach based on evolutionary optimization [**13**]. The study of Cervera and Baños is credited among the first ones that adopt this solution method for the synthesis of a robust controller, but in reference [**13**] the approach was applied to a benchmark example only, and no response constraints in the time domain were considered.

A few applications of evolutionary algorithms (EA's) in the framework of aerospace applications of control theory have been proposed in recent years. Menon *et al.* [**14**] compared the application of different evolutionary optimization methods to the clearance of non-linear flight control laws for highly augmented aircraft. The control law is assumed as given and the analysis is focused on manoeuvre performance evaluation rather than control law synthesis. The comparison with deterministic approaches for the same flight control law clearance problem [**15**] proved that the global optimization methods allows for clearance of the flight control law over continuous regions of the flight envelope in the presence of continuous variations of several aircraft parameters, thus avoiding limitations of current industrial flight clearance process, where only a prescribed set of combinations of the uncertain parameters are checked over a gridding of points within the aircraft flight envelope. Bourmistrova and Khantsis [**16**] adopted an EA as a means for fine tuning robust control laws for unmanned vehicles in the framework of a demanding control task, such as ship deck recovery of a fixed wing UAV. Again, a controller is assumed as a starting point for the analysis, but the EA allows for optimizing the gains in order to improve overall system performance. In this respect, this is, to the authors' knowledge, one of the first attempts of control gain synthesis by means of an EA.

This study proposes an EA as a viable alternative to LMI's for directly solving the minimization process for enforcing frequency domain requirements on robustness and noise abatement, simultaneously (i) enforcing time-domain constraints on the closed-loop behaviour of the system, while (ii) fulfilling different (and possibly competing) requirements in different operating points for the considered plant, when necessary. This is done, as stated before, for a realistic applicative scenario, that is, full-authority longitudinal control of a high-performance jet aircraft.

Gains obtained at convergence by means of the proposed approach always represent feasible controllers, where issues related to time-domain behaviour such as rise time, overshoot, and settling time are addressed during the synthesis process, possibly including the effects of non-linear terms in actuator dynamics (such as position and rate saturation). Moreover, evolutionary algorithms provide a considerable advantage over classical gradient-based optimization algorithms, where a global minimum is sought for problems featuring complex shape of the objective function and/or of the feasible solution region in the search space, at the cost of a considerable computational burden.

Highly manoeuvrable aircraft control offers a particularly challenging scenario, where a controller synthesized for a single trim condition will unlikely perform sufficiently well over a wide portion of the operating envelope, even when robust techniques are used for its synthesis. In this respect, the classic solution is to use gain scheduled controllers, where gains are varied as a function of reference parameters for the flight condition (e.g. Mach number or dynamic pressure). This classical procedure allows for adapting the system to parameter variations, but still requires a certain degree of robustness when the aircraft is flying off-nominal conditions between the design points where the controllers were synthesized or when aggressive manoeuvres are performed, with large variations of the angle of attack. In this framework, a gain scheduled controller for an F-16 fighter aircraft reduced short period model will be derived. The F-16 offers a good test benchmark for the technique as it features most of the characteristics of a modern jet fighter (instability, high-α flight, command augmentation, etc.) [**17**].

In a previous study [**18**], a gain-scheduled controller designed starting from three different trim conditions was compared with a single robust controller derived by enforcing simultaneously the requirements in all the considered operating points by means of a multi-objective optimization approach. As a matter of fact, the wide variation of system parameters over the whole flight envelope did not allow for the determination of a single controller fulfilling all the requirements, so that a converged solution for the optimization process was found only by relaxing some of the constraints. In this respect, some form of gain scheduling appears to be necessary, if the same level of handling qualities is expected over the whole flight envelope. At the same time,

in most aeronautical applications, the dynamic pressure $Q = 0.5\rho V^2$ is used as the scheduling parameter, whereas different dynamic characteristics may be found flying at the same Q but at different altitudes.

The aim of this study is thus twofold. On one side, the preliminary analysis presented in reference [**18**] will be reconsidered and completed synthesizing the control gains by means of an estimation of distribution algorithm (EDA) as the scheduling parameter is varied. In this framework, a single-objective constrained optimization process will be stated (S.O. Problem), where the weighted combination of the infinite-norm of the sensitivity function (for disturbance attenuation requirements) and complementary sensitivity function (for robust stability requirements) must be minimized and attain a value below unity.

The second objective is to exploit the capabilities of the multi-objective search to identify the best controller for different flight conditions corresponding to the same value of the scheduling parameter. A second multi-objective optimization problem is thus defined (M.O. Problem), where a front of optimal feasible solutions is sought, in order to minimize simultaneously the weighted combination of the sensitivity and complementary sensitivity functions for two different flight conditions corresponding to the same value of the dynamic pressure at different flight altitudes. Together with the inherent robustness provided by the H_∞ control approach, this should allow for a truly performing control system over a wider portion of the flight envelope.

The application of H_∞ synthesis method to a rather standard single-input/single-output (SISO) inner-loop control problem represents a preliminary but fundamental step in assessing the capabilities of MOEA in this framework. The application of the technique is completed by the design of an outer auto-pilot loop, with speed-hold and altitude-hold capabilities, by means of a feedback on elevator and throttle. This second MIMO problem completes the synthesis of the full-authority longitudinal control system, thus demonstrating the viability of the approach for both high- and low-bandwidth control tasks typical of aeronautical applications.

One may argue that classical approach to HQ rating is based on frequency domain techniques, but the problems and limits of this approach when dealing with modern, high-performance multi-role aircraft have been questioned and discussed [**1**]. In this respect, the so-called 'modern control theory' [**2**] is based on synthesis processes and requirements defined in the time domain. Moreover, in the framework of this study time-domain specifications also allow for testing closed-loop performance on a complete, fully non-linear model. It is thus possible to analyse aggressive manoeuvres, a possibility not available when dealing with frequency-domain specifications that require a linear system and are thus limited to small displacements from a given trim condition.

After the description of aircraft model and control system architecture and a brief review of H_∞ control theory in the next section, the major features of the optimization method used for solving the control problem are briefly recalled in section 3. The synthesis of a set of controllers in the neighbourhood of several trim conditions to be used for gain scheduling, the evaluation of their off-nominal performance and the analysis of controllers synthesized for different competing merit functions at different trim points is then carried out and discussed in section 4. Numerical simulation is used for testing closed-loop response of the scheduled controller by means of a complete longitudinal non-linear aircraft model. This analysis includes a Montecarlo simulation over 100 different initial trim conditions, randomly generated within the considered portion of the flight envelope. A section of conclusions ends the paper.

2 AIRCRAFT MODEL AND CONTROL SYSTEM ARCHITECTURE

2.1 Equations of motion and simplifications

The longitudinal equations of motion of a rigid aircraft are expressed by a set of four ordinary differential equations in the form

$$\begin{aligned} \dot{U} &= -qW - g\sin\Theta + \left(0.5\rho V^2 S C_x + T\right)/m \\ \dot{W} &= qU + g\cos\Theta + 0.5\rho V^2 S C_z/m \\ \dot{q} &= 0.5\rho V^2 S\bar{c} C_m/I_y \quad ; \quad \dot{\Theta} = q \end{aligned} \tag{1}$$

where the state variables are the velocity components U and W (with $V^2 = U^2 + W^2$), the pitch angular velocity q and the pitch angle Θ. The control variables are the elevator deflection δ_E (which acts on the pitch moment aerodynamic coefficient C_m, but it affects the force coefficients C_x and C_z as well) and the throttle setting δ_T, such that the thrust delivered by the engine is expressed as $T = T_{\max}(h, M)\delta_T$, when engine dynamics is neglected.

Once a trim condition is determined, it is possible to linearize the equations of motion in its neighbourhood by use of a set of stability axes [**19**]. For a level flight condition at velocity V_0, such that

$q_0 = 0$, one gets a fourth-order linear system in the form

$$\begin{pmatrix} \dot{u} \\ \dot{w} \\ \dot{q} \\ \dot{\theta} \end{pmatrix} = \begin{bmatrix} X_u & X_w & X_q & -g \\ Z_u & Z_w & V_0 + Z_q & 0 \\ M_u & M_w & M_q & 0 \\ 0 & 0 & 1 & 0 \end{bmatrix} \begin{pmatrix} u \\ w \\ q \\ \theta \end{pmatrix} + \begin{bmatrix} X_{\delta_E} & X_{\delta_T} \\ Z_{\delta_E} & 0 \\ M_{\delta_E} & 0 \\ 0 & 0 \end{bmatrix} \begin{pmatrix} \Delta\delta_E \\ \Delta\delta_T \end{pmatrix} \tag{2}$$

where the state variables are perturbations of velocity components, u and w, pitch angular velocity, q, and pitch angle, θ. Note that for a rectilinear flight trim conditions q represents both the absolute value of the pitch rate and its perturbation. The control variables are variations of elevator deflection $\Delta\delta_E$ and throttle setting $\Delta\delta_T$ with respect to trim settings, δ_{E_0} and δ_{T_0}. The stability derivatives in equation (2) depend on the considered flight condition. This means that the response of the aircraft to control action will depend on trim speed V_0 and altitude h.

Long-term dynamics do not affect significantly aircraft handling qualities and a reduced order, short-period model is usually sufficient for control law synthesis [**2**], as attitude variables (q and $\alpha \approx w/V_0$) respond to control inputs on δ_E on a faster time scale with respect to trajectory ones (namely velocity V and flight path angle γ, where for longitudinal flight it is $\gamma = \theta - \alpha$). This means that V and γ can be considered approximately constant during a short-term attitude manoeuvre and a reduced-order model given by

$$\begin{pmatrix} \dot{\alpha} \\ \dot{q} \end{pmatrix} = \begin{bmatrix} Z_\alpha/V_0 & 1 + Z_q/V_0 \\ M_\alpha & M_q \end{bmatrix} \begin{pmatrix} \alpha \\ q \end{pmatrix} + \begin{bmatrix} Z_{\delta_E}/V_0 \\ M_{\delta_E} \end{bmatrix} \delta_E \tag{3}$$

is sufficient for describing the most relevant features of aircraft response to elevator inputs.

Model fidelity is enhanced by including actuator and engine dynamics. A first-order response is assumed for the elevator deflection to pilot or automatic control inputs, $\delta_{E_{\text{com}}}$

$$\dot{\delta}_E = \frac{1}{\tau_A}\left(\delta_{E_{\text{com}}} - \delta_E\right) \tag{4}$$

where τ_A is the hydraulic actuator time constant. Both position ($|\delta_E| \leqslant \delta_{E_{\max}} = 25^\circ$) and rate saturation ($|\dot{\delta}_E| \leqslant \dot{\delta}_{E_{\max}} = 60^\circ/\text{s}$) are accounted for in the actuator model. When the complete longitudinal model is considered, also engine dynamics is included in the form of a first-order lag, with a time constant $\tau_E = 5\,\text{s}$. Saturation level for throttle setting are between 0 (idle) and 1 (full thrust with afterburner).

In what follows, an F-16 fighter aircraft model will be considered [**2**], that features an aerodynamic database for $-10 \leqslant \alpha \leqslant 45^\circ$ and $|\beta| \leqslant 30^\circ$. The set of four non-linear ordinary differential equations in equation (1) will be used for numerical simulation at the end of section 4. A sequential-quadratic programming algorithm is adopted for determining the reference trim conditions for the control law synthesis. Finite differences are used to linearize the aircraft model in the neighbourhood of each trim condition and obtain the stability derivatives for equation (3).

2.2 Architecture of the longitudinal control system

As stated in section 1, the longitudinal control system architecture is based on a two-level nested architecture, featuring an inner stability and control augmentation loop and an outer loop for auto-pilot functions. The architecture is depicted in Fig. 1, where the nested structure is clearly visible. The inner loop deals with fast attitude variables, α and q, where a super-augmentation system allows to track pilot commands on pitch angular speed. The outer loop deals with slow trajectory variables, where deviations from the desired values provided by two reference signals for velocity V and climb angle γ are compensated. Details are provided in the next subsections.

2.3 Longitudinal SCAS

Figure 2 depicts the structure of a longitudinal SCAS. The blocks P and A represent the aircraft and elevator actuator dynamics, respectively. The stability augmentation provides increased pitch damping (by q-feedback) and artificial static stability (α feedback). In this latter case, a filter, $F(s) = \tau_F/(s + \tau_F)$, is included for reducing α sensor noise, with a cut-off frequency of $\tau_F = 10\,\text{rad/s}$.

The control augmentation system transforms the longitudinal pilot command into a rate command, where the tracked variable is the pitch angular velocity q. In order to provide the system with zero steady-state error an integrator is included in the pitch angular velocity error channel. The resulting open loop dynamics (including the α filter and the integrator variable ε, such that $\dot{\varepsilon} = r_q - q$) is described by a linear system of ordinary differential equations in the form

$$\dot{\boldsymbol{x}} = \boldsymbol{A}\boldsymbol{x} + \boldsymbol{B}u\,; \quad \boldsymbol{y} = \boldsymbol{C}\boldsymbol{x} \tag{5}$$

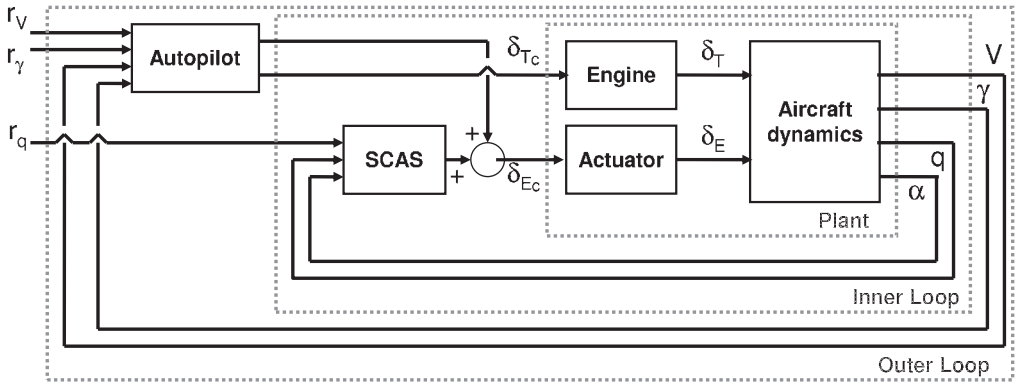

Fig. 1 Control system architecture

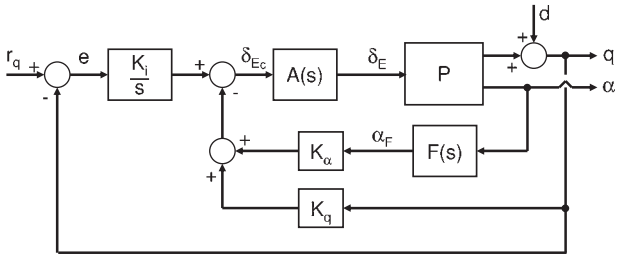

Fig. 2 Longitudinal stability and control augmentation system

where the state vector is $\boldsymbol{x} = (\alpha, q, \delta_E, \alpha_F, \varepsilon)^T$, while the only input variable is the pitch velocity reference signal r_q. Provided that the output variables are $\boldsymbol{y} = (\alpha, q, \varepsilon)^T$, the state, control, and output matrices are defined as

$$\boldsymbol{A} = \begin{bmatrix} Z_w & V_0 + Z_q & M_{\delta_E} & 0 & 0 \\ M_w & M_q & M_{\delta_E} & 0 & 0 \\ 0 & 0 & -\tau_A & 0 & 0 \\ 0 & 0 & 0 & -\tau_F & 0 \\ 0 & -\frac{180}{\pi} & 0 & 0 & 0 \end{bmatrix}; \quad \boldsymbol{B} = \begin{bmatrix} 0 \\ 0 \\ \tau_A \\ 0 \\ 0 \end{bmatrix}$$

$$\boldsymbol{C} = \begin{bmatrix} \frac{180}{\pi} & 0 & 0 & 0 & 0 \\ 0 & \frac{180}{\pi} & 0 & 0 & 0 \\ 0 & 0 & 0 & 0 & 1 \end{bmatrix} \tag{6}$$

respectively. The gains of the stability augmentation system (K_α and K_q) and the integral gain (K_i) will be determined by means of an optimization algorithm in the framework of H_∞ control theory for the reduced order short-period aircraft model, including elevator dynamics and α-filter.

2.4 Autopilot functions

The autopilot features two functions: a velocity hold and an altitude hold. In the first case, a proportional–integral (PI) feedback on the velocity error is adopted in order to regulate the value of airspeed to the reference signal provided by the pilot. In the second case, a reference $\gamma_{des} = 0$ is provided for the climb angle to the auto-pilot. Again, a PI network is considered in order to regulate to zero the error on the climb angle, thus forcing the aircraft in a flight at constant altitude. Note that, for a linear longitudinal model, this corresponds (under a simple scaling of control system gains) to a feedback on altitude and climb rate, that is, a proportional-derivative feedback on altitude changes.

A standard piloting technique is adopted, where the velocity hold function provides an increment to the elevator command, while the altitude hold function drives variations in throttle commands (Fig. 1). A total of four gains need to be identified for the two input–two output system thus obtained, where the controlled plant is represented by the augmented aircraft longitudinal dynamics. The complete, four variable linear longitudinal model is considered, including a first-order engine response to throttle commands.

2.5 Robust control

Consider the system depicted in Fig. 3, where $\boldsymbol{P}_0(s)$ is the nominal model of a plant with n_i inputs and n_o outputs, $\boldsymbol{C}(s)$ the controller, $\boldsymbol{r}(s)$ the reference input signal that needs to be tracked by the output $\boldsymbol{y}(s)$, $\boldsymbol{d}$ the noise on the output signal, and $\boldsymbol{n}$ the noise on the sensors. Given the definition of the output transfer matrix as $\boldsymbol{L}_o = \boldsymbol{P}_0\boldsymbol{C}$, the sensitivity at the output is defined as the transfer matrix $\boldsymbol{y}/\boldsymbol{d}$, that is

$$\boldsymbol{S}_o = (\boldsymbol{I} + \boldsymbol{L}_o)^{-1}, \quad \boldsymbol{y} = \boldsymbol{S}_o\boldsymbol{d} \tag{7}$$

and the complementary sensitivity function at the output is

$$\boldsymbol{T}_o = \boldsymbol{I} - \boldsymbol{S}_o = \boldsymbol{L}_o(\boldsymbol{I} + \boldsymbol{L}_o)^{-1} \tag{8}$$

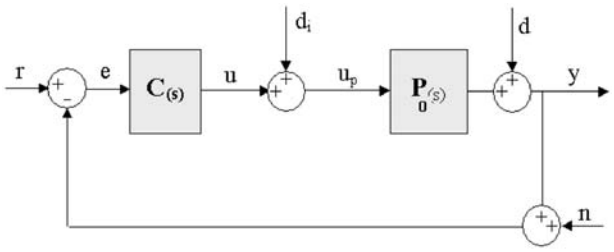

Fig. 3 General feedback configuration with disturbances

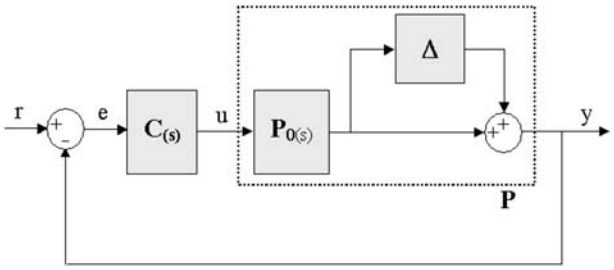

Fig. 4 Feedback configuration with multiplicative uncertainties on the nominal model

From the system represented in Fig. 3, the output can be expressed as

$$\boldsymbol{y} = \boldsymbol{T}_o\boldsymbol{r} - \boldsymbol{T}_o\boldsymbol{n} + \boldsymbol{S}_o\boldsymbol{P}\boldsymbol{d}_i + \boldsymbol{S}_o\boldsymbol{d} \tag{9}$$

It is thus clear that in order to eliminate or at least reduce the effects of noise on the response of the system, it is necessary to operate on $\boldsymbol{T}_o$ and $\boldsymbol{S}_o$.

Moreover, apart from external noises affecting the signals, the system may be characterized by other kinds of uncertainties. Usually, the nominal model $\boldsymbol{P}_0$ does not correspond to the actual plant, due to simplifying assumptions and/or linearization. Taking into account a multiplicative uncertainty on the plant model (Fig. 4), the following expression for the output is obtained

$$\boldsymbol{y} = \frac{\boldsymbol{T}_o + \Delta\boldsymbol{T}_o}{\boldsymbol{I} + \Delta\boldsymbol{T}_o}\boldsymbol{r} \tag{10}$$

In order to reduce the effect of the uncertainty, it is necessary to tailor the complementary sensitivity function of the uncertainty itself, $\Delta\boldsymbol{T}_o$.

The main idea behind H_∞ control theory and the design process derived in this framework is to find the values of the controller parameters by minimizing appropriately the infinite norm of the weighted sensitivity and complementary sensitivity functions. In order to achieve this result, the following functions need to be minimized

$$\|\boldsymbol{W}_1(s)\boldsymbol{S}_o(s)\| = \min; \quad \|\boldsymbol{W}_3(s)\boldsymbol{T}_o(s)\| = \min \tag{11}$$

that is, the effects of noise on the output and that of uncertainties of the nominal model $\boldsymbol{P}_0$ are reduced, $\boldsymbol{W}_1(s)$ and $\boldsymbol{W}_3(s)$ being weighting functions chosen during the design as a function of expected disturbances and uncertainties and requirements on closed-loop performance.

Since the H_∞ norm of a system $\boldsymbol{G}(s)$ is

$$\|\boldsymbol{G}\|_\infty = \sup_\omega \bar{\sigma}\big[\boldsymbol{G}(j\omega)\big] \tag{12}$$

where $\bar{\sigma}(\cdot)$ is the maximum singular value, this kind of norm provides the worse gain for a sinusoidal input at a given frequency, corresponding to the worse energetic gain of the system. The use of weighted functions allows to deal with different kinds of signals, when MIMO systems are considered. Moreover, and more important, weights allow to focus the optimization process only within prescribed frequency ranges. As an example, in order to reduce low frequency noise a weight function with high gains at low frequency will be used, such that

$$\|\boldsymbol{W}_g(s)\boldsymbol{G}(s)\|_\infty < 1 \implies |G_{ij}(s)| < \frac{1}{|W_{g_{ij}}(s)|} \tag{13}$$

that is, the magnitude of each transfer function from input i to output j is less than the inverse of the magnitude of the corresponding weight.

3 CONTROL LAW SYNTHESIS

As stated in section 1, evolutionary optimization algorithms offer an advantage over gradient-based methods, that can hardly be applied when constraints make the shape of the feasible solution subset of the search space highly irregular. The particular type of evolutionary algorithm used for tackling the considered control problem belongs to the subclass of EDAs [**20**]. In general terms, these methods try to identify a probabilistic model of the search space from the results for the current populations. Crossover and mutation operators, typical of classical genetic algorithms [**21**], are replaced with statistical sampling [**22**].

3.1 The evolutionary optimization algorithm

The MOPED (multi-objective Parzen-based estimation of distribution) algorithm is a multi-objective optimization algorithm for continuous problems that use the Parzen method to build a probabilistic representation of Pareto solutions, with multivariate dependencies among variables [**23**, **24**]. Similarly to what was done in reference [**22**] for multi-objective Bayesian optimization algorithm (moBOA), some techniques of NSGA-II are used to classify promising

solutions in the objective space, while new individuals are obtained by sampling from the Parzen model. NSGA-II was identified as a promising base for the algorithm mainly because of its intuitive simplicity coupled with excellent results on many problems.

The Parzen method [**23**] pursues a non-parametric approach to kernel density estimation and it gives rise to an estimator that converges everywhere to the true probability density function (PDF) in the mean square sense. Should the true PDF be uniformly continuous, the Parzen estimator can also be made uniformly consistent. In short, the method allocates N_{ind} identical kernels (where N_{ind} is the number of individuals of the population of candidate solutions), each one centred on a different element of the sample.

MOPED demonstrated in the past its effectiveness in handling constrained problems, and will be used here to assess the validity of the control synthesis technique. The efficiency of the solver is not the focus of this research. Nonetheless, a comparison among different evolutionary optimization methods will be addressed in the future in order to evaluate the best suited approach for the application to H_∞ control problems in terms of efficiency and capability of finding different, possibly distant, feasible zones. The peculiar aspects of MOPED with respect to the more popular NSGA-II are recalled in the sequel.

3.1.1 Classification and fitness evaluation

The individuals of the population are classified in a way that favours the most isolated individuals in the objective function space, in the first subclass (highest dominance) of the first class (best suited with respect to problem constraints). If the problem is characterized by m constraints $c_i(\boldsymbol{x})$, $i=1, 2, \ldots, m$, such that $c_j(\boldsymbol{x})=0$ indicates that the jth constraint is satisfied, the first step in the evaluation of the fitness parameter is the determination of the degree of compatibility of each individual with the constraints. The compatibility, indicated by the symbol cp, is measured as the weighted sum of unsatisfied constraint. Once the value of cp is evaluated for all the individuals, the population is divided in a predetermined number of classes, $1+N_{cl}$. The N_{best} individuals that satisfy all the constraints, such that $cp=0$, are in the first class. The remainder of the population is divided in the other groups, each one containing an approximately equal number of individuals, given by round $(N_{ind}-N_{best})/N_{cl}$.

The second class is formed by those individuals with the lower values of the constraint parameter and the last one by those with the highest values. For each class, individuals are ranked in terms of dominance criterion and crowding distance in the objective function space, using the NSGA-II techniques. After ranking all the individuals of the population, from the best to the worst one, depending on their belonging to a given class and dominance level and the value of their crowding parameter, a fitness value f is assigned to each individual.

3.1.2 Building the model and sampling

The fitness value determines the weighting of the kernel for sampling the individuals of the next generation. As an example, if f is linearly varying from $2-\alpha_f$ (best individual of the entire population) to α_f (worst individual), with $\alpha_f \in [0;\ 1)$, for $\alpha_f=0$, the best solution ($f=2$) provides a kernel with twice as much possibilities of generating new individuals for the next generation than the central one, placed at half of the classification (for a corresponding value of $f=1$), while the kernel for the worst one ($f=0$) is prevented from generating new individuals. f distribution is then normalized to have $\sum_{i=1,\ldots,N_{ind}} f=1$.

By means of the Parzen method, a probabilistic model of the promising search space portion is thus built on the basis of the information given by N_{ind} individuals of the current population, and $\tau_E N_{ind}$ new individuals ($\tau_E \geqslant 1$) can then be sampled. The variance associated to each kernel depends on (i) the distribution of the individuals in the search space and (ii) the fitness value associated to the pertinent individual, so as to favour sampling in the neighbourhood of the most promising solutions. In order to improve the exploration of the search space, it is sometimes useful to alternatively adopt two different kernels when passing from one generation to the following one.

3.2 Statement of the optimization problems

3.2.1 S.O. Problem for inner-loop SCAS

The single-objective optimization process is aimed at minimizing the function F, equal to a weighted sum of the sensitivity and complementary sensitivity functions. The objective function is thus expressed as

$$F = \|W_1(s)S(s)\|_\infty + \|W_3(s)T(s)\|_\infty \tag{14}$$

The weight functions are

$$W_1 = \frac{s+100}{100s+1}; \qquad W_3 = \frac{100s+10}{s+1000} \tag{15}$$

where W_1 is chosen, so that the action on the sensitivity function is emphasized in the low frequency range, where the effect of disturbances may affect aircraft performance, while W_3 is tailored on the

basis of assumed characteristics for the uncertainties on the nominal model of the plant. Sensitivity, complementary sensitivity and weights are scalar functions for the considered SISO problem.

The design variables are the three gains of the SCAS (Fig. 2), namely K_α, K_q, and K_i. The resulting three-dimensional search domain is bounded by $\boldsymbol{lb} = (-5, -5, -5)^T$ and $\boldsymbol{ub} = (0, 0, 0)^T$. However, the search space is normalized and the solver operates in the cube $[0, 1] \times [0, 1] \times [0, 1] \subset \mathbb{R}^3$.

Constraints on peak time t_p, settling time t_s, and overshoot M_p are also included, representative of requirements on handling qualities. Feasible solutions must thus satisfy the following inequality constraints

$$\begin{aligned} &t_p \leqslant 1\text{s}; \quad t_s \leqslant 3\text{ s}; \quad M_p \leqslant 0.05; \\ &\|W_1(s)S(s)\|_\infty \leqslant 1; \quad \|W_3(s)T(s)\|_\infty \leqslant 1 \end{aligned} \tag{16}$$

The S.O. problems were first solved on a denser set of trim points, between those tested in reference [**18**], and a gain scheduled controller was thus developed. A more detailed analysis was then performed for two pairs of trim points at $h = 0$ and $h = 12\,000$ ft, each pair corresponding to the minimum and maximum values of the dynamic pressure, respectively.

3.2.2 M.O. Problem for inner-loop SCAS

In the second approach, a bi-objective optimization process is carried out for each pair of points with the same dynamic pressure. In this case, the solver searches for solutions, which optimize the objective functions F_1 and F_2 simultaneously for the two considered trim points, while enforcing the time-domain constraints for both of them.

3.2.3 M.O. Problem for MIMO outer-loop autopilot functions

In this case, a bi-objective optimization process is carried out for a specified operating point, which corresponds to point A1 in Table 1. The objective functions are

$$F_1 = \|W_1(s)\boldsymbol{S}_d(s)\|_\infty; \quad F_2 = \|W_3(s)\boldsymbol{T}(s)\|_\infty \tag{17}$$

Table 1 Trim conditions

	V (ft/s)	h (ft)	Q (psf)
A1	500	0	297
A2	600	12 000	297
B1	748	0	666
B2	900	12 000	666
T1	736	24 000	297
T2	821	30 000	297
T3	700	6000	486

where $\boldsymbol{S}_d(s)$ is the matrix composed by the diagonal elements of the sensitivity matrix and $\boldsymbol{T}(s)$ the complementary sensitivity matrix, respectively, and the weights are

$$W_1 = \frac{s+5}{50+1}; \quad W_3 = \frac{100s+10}{s+1000} \tag{18}$$

The design variables are the four gains of the autopilot, K_{p_V}, K_{i_V}, K_{p_G}, and K_{i_G}. The resulting four-dimensional (4D) search domain is bounded by $\boldsymbol{lb} = (0, 0, 0, 0)^T$ and $\boldsymbol{ub} = (15, 15, 30, 15)^T$. Also, in this case, the search space is normalized and the solver operates in 4D hypercube with edges $[0, 1] \subset \mathbb{R}$.

Constraints on overshoot M_{pV} on velocity, and stationary precisions on velocity and flight-path angle (δV and $\delta\gamma$, respectively) are also included for a step variation ΔV_{des} of velocity, with $\Delta\gamma_{\text{des}} = 0$ for the flight-path angle. Feasible solutions must thus satisfy the following inequality constraints on time domain responses

$$M_{pV}/\Delta V_{\text{des}} \leqslant 0.1; \quad \delta V/\Delta V_{\text{des}} \leqslant 0.1; \quad \delta\gamma_{des} \leqslant 0.001^\circ \tag{19}$$

and on frequency domain response

$$\|W_1(s)\boldsymbol{S}_d(s)\|_\infty \leqslant 1; \quad \|W_3(s)\boldsymbol{T}(s)\|_\infty \leqslant 1 \tag{20}$$

Note that, in this case, the enforcement of time domain constraints was not dictated by the need of the applicative scenario, where time response is not an issue, for low-band width autopilot tasks. Rather, the requirements were placed in order to test the capabilities of the considered control synthesis technique for a MIMO M.O. case.

3.2.4 Algorithm parameters and numerical performance

The parameters to be set for the MOPED algorithm are: size of the population, N_{ind}, number of constraint classes, N_{cl}, the fitness parameter, α_f, and the sampling proportion, τ_E. In all the optimization processes for this study, the following parameter values were used: $N_{ind} = 100$, $N_{genMAX} = 100$, $N_{cl} = 3$; $\alpha_f = 0.5$; $\tau_E = 1$.

Although EA's are computationally demanding, the resulting numerical performance allows for a rather efficient synthesis process. The optimization algorithm running on a standard PC with processor INTEL - T7500 with 2.2 GHz requires on average a computational time of 19 min for the single-point optimization and 40 min for the double-point optimization. Autopilot case needs 45 min, but in this case the long computational time is mainly due to the need for longer simulation interval up to 100 s, when low-bandwidth tasks are considered.

A simulation time of only 50 s was considered in all the other cases.

4 RESULTS

In what follows, a review of the major findings obtained by solving the H_∞ control problem by means of an evolutionary optimization approach will be summarized. As stated in section 1, some preliminary results were obtained in a previous work [**18**], where only a reduced number of trim points was considered. The approach proved to be effective in tackling the H_∞ minimization problem for the SISO inner loop, but several problems remained open that will be addressed in the sequel. As a further contribution, a MIMO autopilot outer loop is synthesized by means of an MOEA, according to the procedure outlined in the previous sections, thus completing the structure of the longitudinal control system for the considered high-performance jet aircraft.

4.1 Inner SISO loop for SCAS

4.1.1 Gain scheduling

The study reported in reference [**18**] demonstrated that it is not possible to devise a single set of values for the control gains, K_i, K_α, and K_q, with adequate performance over a large portion of the flight envelope. By exploiting the multi-objective approach, the minimization problem was simultaneously considered at three different trim conditions (low, medium, and high speed at increasing altitudes, x symbols in Fig. 5), but the strong variation of stability and control derivatives with dynamic pressure (particularly significant for the most important control derivative, M_{δ_E}) prevents the algorithm from finding a compromise between high control power (and resulting small deflections) at high speed and weaker control effectiveness at low speed.

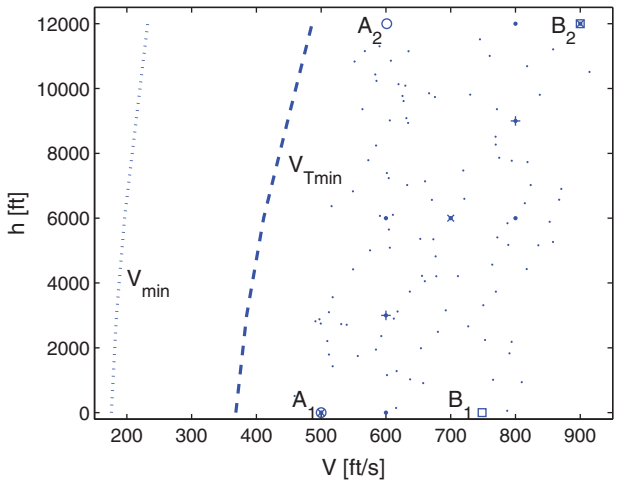

Fig. 5 Control law design and test trim points in the F-16 flight envelope

When the nominal values of the time-domain constraints were considered, it was not possible to obtain convergence of the optimization process to feasible controllers that satisfy time-domain constraints with an H_∞ norm less than 1 in all the design points. At the same time, for those values of K_i, K_α, and K_q resulting in a robust controller, time-domain requirements where violated at least for one of the design trim conditions. Only by relaxing time-domain constraints, thus allowing a higher overshoot and/or a longer rise-time, an acceptable controller that satisfies the necessary condition for robustness was obtained. These results were further confirmed by analysis of the closed-loop system response to a step input in two test points, at airspeeds of 600 and 800 ft/s and altitudes equal to 3000 and 9000 ft, respectively (+ symbols in Fig. 5).

After the preliminary application described in reference [**18**], a more detailed analysis of the variation of controller gains for different values of the scheduling parameter Q is now considered. A set of nine design points were selected (• symbols in Fig. 5) and the optimal gains were identified by means of a single-objective evolutionary optimization process. Note that all the points lie in the region where thrust necessary for level flight increases with velocity (that is, to the right of the minimum-thrust trim flight condition in the h–V flight envelope), in a range of altitudes between sea level and approximately one-fourth of the aircraft service ceiling, rated around 50 000 ft. The considered analysis will be limited to the subsonic velocity range, as compressibility effects are neglected in the aircraft aerodynamic model.

The variation of the obtained controller gain is relatively smooth, as shown in Fig. 6. The stability augmentation system needs an almost constant gain K_α throughout the considered interval of Q, while significant adjustments to the pitch damper and command augmentation gains K_q and K_i are required. Both K_q and K_i are almost exactly inversely proportional with respect to Q: a variation from -0.56 to -0.24 is required for K_q, and between -1.72 and -0.75 for K_i, with a ratio equal to 2.33 for the first one and 2.29 for the second, that almost exactly matches the ratio $Q_{\max}/Q_{\min} = 2.24$.

This type of variation can be explained on physical grounds, when one considers that the angle of attack α remains well within the linear aerodynamic range, throughout the considered portion of the flight envelope, and the variation of the gains is mainly driven by

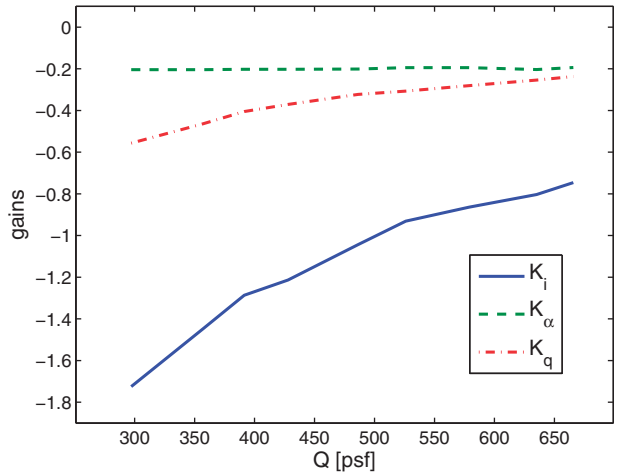

Fig. 6 Control law design and test trim points in the F-16 flight envelope

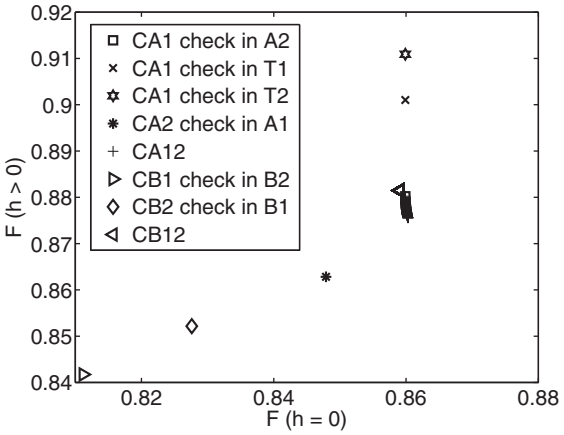

Fig. 7 Pareto front approximations and cross-checking

control power, which is proportional to the dynamic pressure Q. In this framework, a robust controller can handle the variations of the dynamic response when aggressive manoeuvres are considered, involving the non-linear terms of the complete aerodynamic model when large variations of α are considered.

4.1.2 *Effects of altitude changes for fixed values of* Q

In order to evaluate the effects of altitude changes for fixed values of Q, four design trim conditions for the F-16 aircraft model were considered (listed in Table 1 and indicated in Fig. 5 as A1, A2, B1, and B2). Three additional trim conditions were used for simulation of the closed-loop behaviour in off-nominal conditions (T1, T2, and T3 in Table 1).

The results obtained from the optimization process in terms of robustness measure are summarized in Fig. 7, while the corresponding values of the constraint parameters are listed in Table 2. In what follows, CA1 is the controller optimized in trim condition A1, CA2 the controller optimized in A2, CA12 is one of the controllers obtained by means of the multi-objective search, when both A1 and A2 trim conditions are considered. In an analogous way, CB1 and CB2 are the controllers optimized in B1 and B2 trim points, respectively, while CB12 is one of the controllers obtained when B1 and B2 flight conditions are considered simultaneously.

The analysis of the results and the cross-checking of the controller behaviour in off-design conditions show that controller scheduling over dynamic pressure may not be sufficient for robust performance and handling qualities, as far as speed and altitude may play a role separately. In particular, if the low

Table 2 Cross-checking of controllers and trim conditions: time-domain constraints on t_p, M_p, and t_s

	t_p	M_p	t_s
CA1 in A2	0.990 802	0.042 508	2.732 465
CA1 in T1	0.955 337	0.053 440	2.750 411
CA1 in T2	0.946 109	0.058 752	2.419 744
CA2 in A1	1.121 142	0.021 026	2.703 230
CB1 in B2	1.036 109	0.031 622	2.635 621
CB2 in B1	0.954 420	0.071 994	3.147 958

dynamic pressure range is considered, controller CA1 behaves well (in terms of both frequency and time-domain constraints) also in A2 (even if the rise time increases and the constraints are enforced only marginally). As a matter of fact, the small Pareto front in Fig. 7 (+ signs) obtained when A1 and A2 conditions are considered together starts from the point corresponding to CA1. It should be noted that the opposite is not true, that is, CA2 fails to work in A1, since the rise time constraint is violated. Moreover, if altitude is further increased (points T1 and T2, not reported in Fig. 5), also the behaviour of CA1 becomes less and less acceptable, with stronger violations of the constraint on overshoot, induced by the reduction of the damping when density gets smaller.

The importance of considering the influence of altitude for a given value of Q appears even more evident when high dynamic pressure conditions are taken into account. Both CB1 and CB2 controllers do not satisfy time domain constraints when checked in the other design point. The difficulties of the control synthesis for high values of Q are also highlighted by the results of the Pareto front related to the search for the CB12 control. In this case, the solver is not able to spread the population over a front of feasible

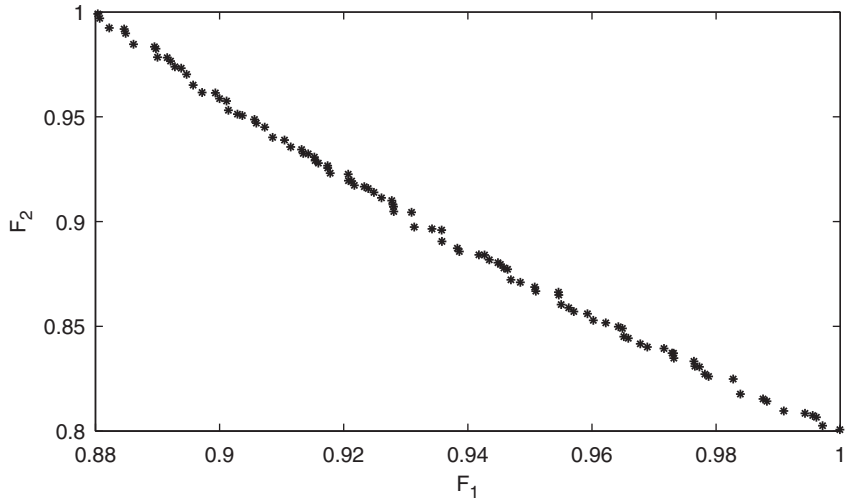

Fig. 8 Pareto front for the synthesis of auto-pilot gains

solutions, rather, it finds a single feasible solution which satisfies constraints in both the design points, but it is characterized by a weaker robustness in both points, if compared with CB1 and CB2.

In order to further validate the approach, a final check was performed in the trim point T3, which has an intermediate value of Q between $Q_{\min}$ and $Q_{\max}$. The controller obtained by linear interpolation between CA12 and CB12 gives following values: $W_1S=0.17134$, $W_3T=0.77243$, $t_p=1.03042$, $M_p=0.010\,19$, and $t_s=2.936\,53$, which means that all the design requirements are met, with only a marginal violation for the rise time, thus confirming on one side the effectiveness of the scheduling method, but at the same time the importance of including the effects of altitude on the model during the design phase.

4.2 Outer MIMO autopilot loop

In this second applicative scenario, the autopilot gains were selected in the trim point labelled as A1 (that is, $V_0=500$ ft/s at sea level ($h=0$). A competitive minimization process between peak values of sensitivity and complementary sensitivity functions, indicated as F_1 and F_2, respectively. In this case, a Pareto front like that reported in Fig. 8 is obtained, where the elements of the considered population of controllers in the top-left corner provide maximum robustness, at the cost of a lower attenuation of low-frequency disturbance, while those lying in the bottom-right region of the plot are less robust to unstructured uncertainties, but provide better attenuation of disturbance in nominal conditions.

One of the feasible controllers obtained from the optimization process was chosen for the analysis in the time domain. The selected gains are $K_{pV}=5.835$, $K_{i_V}=1.955$, $K_{p_G}=17.687$, and $K_{i_G}=2.073$. A step command on the velocity is considered as the input to the closed-loop system, equal to 10 per cent of the current trim speed. The resulting variations of velocity ΔV, angle of attack, α, climb and pitch angles, γ and θ are reported in Fig. 9, where it is possible to appreciate how the auto-pilot rapidly drives the aircraft to the desired flight speed, with only minor residual phugoid oscillations (less than 0.5° in amplitude during the initial transient). The automatic throttling system rapidly cancels the climb rate and successfully maintains the current altitude, with an error of only 6 ft, approximately.

4.3 Analysis of short-period closed-loop response

As a final check for the validity of the proposed approach in the synthesis of robust control laws with respect to reasonable variations of plant dynamics, two sets of simulations were performed. The first set of simulations is based on the analysis of closed-loop response of a complete longitudinal model, thus including the effects of velocity and climb angle variations, which were not accounted for in the design phase, where only a reduced-order short-period model was considered. A second set of simulations was performed, starting from 100 different randomly generated trim points, within the considered region of the flight envelope. It is thus possible to test the closed-loop system on a sufficiently large number of off-nominal conditions, significantly different in terms of altitude and/or flight speed from the trim points adopted for the control law synthesis process.

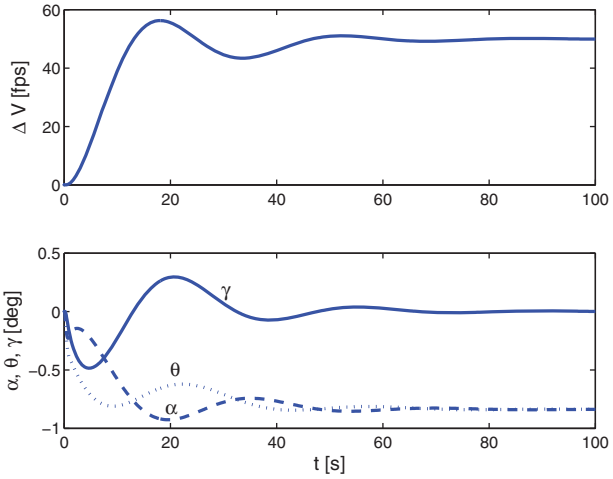

Fig. 9 Response of the auto-pilot to a step-command on V ($\Delta V_{\text{des}} = 50$ ft/s)

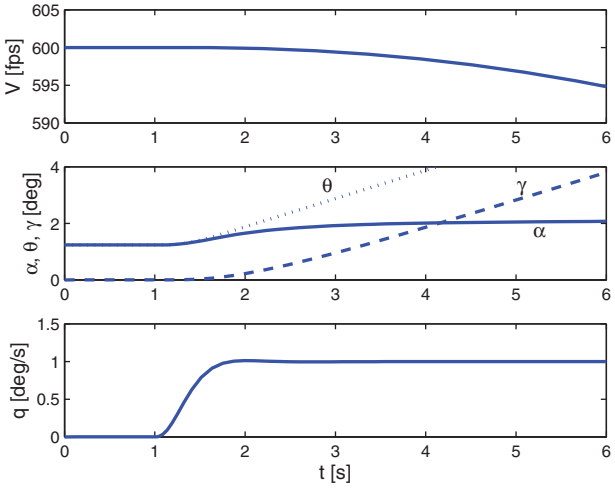

Fig. 10 Non-linear model response to a step input ($r_q = 1°/\text{s}$)

4.3.1 *Non-linear simulation*

A fully non-linear dynamic model of the aircraft is here considered, in order to test if neglected dynamic characteristics (that is, long-term dynamics and inertial and aerodynamic non-linearities) affect closed loop behaviour. In this respect, the non-linear aerodynamic model, where aerodynamic coefficients are tabulated as a function of aerodynamic angles and control surface deflection, further challenges the robustness of the SCAS, when aggressive manoeuvres are simulated, featuring large variations of α. Two manoeuvres are considered, starting from the same trim condition, namely T3, in order to consider an off-design reference point.

When a unity step on the input channel is considered (Fig. 10), the resulting manoeuvres involve a mild variation of pitch angular velocity and angle of attack. The behaviour of the non-linear model resembles almost perfectly that of the linear one, used for the synthesis process. In the short term, rise and settling times and overshoot match the values obtained for the linear case, and only minor differences are present at the end, because of the reduction of velocity and increase in the flight-path angle, γ.

These phenomena are enhanced in the second manoeuvre (Fig. 11), where a more aggressive pilot input is considered, with a sequence of two impulses on the desired pitch angular speed channel, with an amplitude of 10°/s and a duration of 5 s each. The duration of the manoeuvre was increased to 20 s in order to evaluate the recovery capabilities of the SCAS, with no further pilot input.

In the first phase ($t < 6$ s), the sudden increase of the angle of attack of almost 10° puts the aircraft on

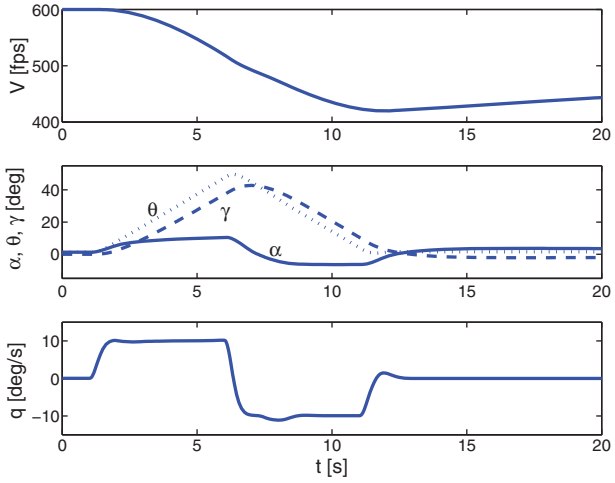

Fig. 11 Non-linear model response to a double impulse ($r_q = 10°/\text{s}$)

a steep-climbing trajectory, so that the velocity rapidly drops, because the manoeuvre was not accompanied by a change in the throttle setting. In spite of this, the command augmentation system successfully tracks the desired value. After 5 s spent at 10°/s of pitch rate, the pitch and climb angles are both around 40°, the pitch angle being larger.

At this point, the command is reversed. Again, the desired variation of q is successfully tracked. The higher overshoot clearly visible at 8 s is related to the variation of stability derivatives over an excursion of α, which varies from more than 10° to less than −5° in less than 2 s. Nonetheless, when the pitch command is brought back to 0, the SCAS successfully start a recovery phase, which ends at the original trim state without requiring any pilot input.

4.3.2 Monte Carlo analysis

Flight conditions in the h–V plane are randomly chosen according to the following rule

$$h = \sigma_h h_{\max}$$
$$V_{eq} = V_{\min} + (V_{\max} - V_{\min})\sigma_V$$

where σ_h and σ_V are random numbers with uniform distribution in the closed interval [0, 1], $h_{\max} = 12\,000$ ft is the maximum altitude considered in the analysis, while maximum and minimum equivalent airspeeds are given by $V_{\min} = 450$ ft/s and $V_{\max}$ 800 ft/s, respectively. Note that maximum and minimum airspeeds lie outside of the speed interval considered for the synthesis of the control law, so that the gains are extrapolated in all those cases that fall outside of the velocity interval considered for the synthesis of the control law.

For a true airspeed $V = V_{eq}\sqrt{\rho_{SL}/\rho(h)}$, aircraft trim is determined in each point, (h, V). $N = 100$ trim points are considered, in order to analyse closed-loop behaviour over a sufficiently large number of off-nominal operating conditions. These points are indicated by thin dots in Fig. 5. Time-domain responses are reported in Fig. 12, which clearly shows how a perfectly stable response is obtained in all the considered conditions, most of which (94 per cent) remain close to the nominal response.

At the same time, a certain degradation is present for six cases, characterized by an overshoot significantly higher than that specified by problem constraints. These critical cases correspond to high-speed conditions, at equivalent velocities significantly higher than V in point B1. The resulting behaviour is caused by an insufficient value of the control gains on the q and α channels, when these are extrapolated from values synthesized at lower speed. The increment in control power at high speed does not compensate the overall reduction of damping and increment of the (positive) static stability derivative M_α, when flying at high altitudes, which cause the unstable pole to become more pronouncedly positive. Note that no degradation is apparent, when the gains are extrapolated at speed lower the minimum one considered for the synthesis.

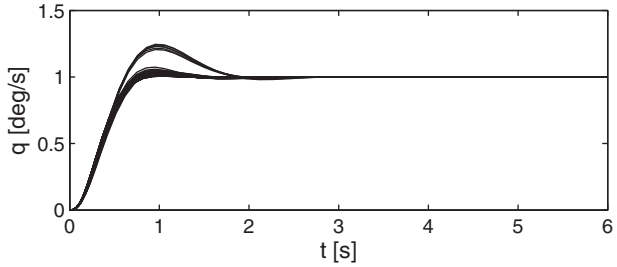

Fig. 12 Monte Carlo analysis of system response in $N = 100$ different trim points ($r_q = 1^\circ$/s)

5 CONCLUSIONS

An evolutionary optimization technique was adopted as a means for control gain synthesis in the framework of H_∞ control problems. Two different approaches were analysed: (a) a single-objective constrained optimization process, where the weighted combination of the infinite-norm of the sensitivity and complementary sensitivity functions were minimized, with constraints on time domain responses, for different trim point conditions; and (b) a bi-objective search where a front of optimal feasible solutions is sought, in order to minimize simultaneously the weighted combination of the sensitivity and complementary sensitivity functions for two different flight conditions, corresponding to the same value of the dynamic pressure at different flight altitudes. A bi-objective search was implemented also for the synthesis of an MIMO auto-pilot system.

The results obtained confirm that the evolutionary approach has an advantage over the more traditional LMI control synthesis technique as it is possible to address time-domain constraints during the synthesis of the control law rather than by means of a trial-and-error technique based on *a posteriori* simulations. More important, once the relevance of stability derivative variation at different altitudes for a fixed value of the scheduling parameter Q is recognized, the bi-objective approach allows for the determination of controllers which perform extremely well in off-nominal conditions, a result which is impossible to obtain by means of control approaches based on local information only. The validity of the approach was confirmed by means of direct simulation of a complete longitudinal non-linear aircraft model and a Monte Carlo analysis over a wide portion of the flight envelope, which includes regions far from the points where the control law syntheasis was performed.

REFERENCES

1 **Abzug, M. J.** and **Larabee, E. E.** *Airplane stability and control: a history of the technologies that made aviation possible*, 1997 (Cambridge University Press, Cambridge), chapter 20.

2 **Stevens, B. L.** and **Lewis, F. L.** *Aircraft control and simulation*, 2nd edition, 2003 (J. Wiley and Sons, New York), chapters 2 and 3.
3 **Avanzini, G.** and **Galeani, S.** Robust antiwindup for manual flight control of an unstable aircraft. *J. Guid. Control Dyn.*, 2005, **28**(6), 1275–1282.
4 **Avanzini, G.** and **De Matteis, G.** Design of a ship-board recovery system for a shrouded-fan UAV. In Proceedings of the 23rd ICAS Congress, Toronto, Canada, September, 2002, Proceedings published on CD-ROM.
5 **Avanzini, G., Ciniglio, U.,** and **De Matteis, G.** Full–envelope robust control of a shrouded–fan unmanned vehicle. *J. Guid. Control Dyn.*, 2006, **29**(2), 435–443.
6 **Zhou, K.** and **Doyle, J. C.** *Essentials of robust control*, 1998 (Prentice-Hall, Englewood Cliffs, New Jersey), chapters 6–9.
7 **Hyde, R. A.** The VAAC Harrier design study. In Proceedings of the AIAA Guidance, Navigation, and Control Conference and Exhibit, Portland, Oregan, USA, 1999, AIAA Paper 99–4278, Proceedings published on CD-ROM.
8 **Smerlas, A., *et al.*** Design and flight testing of an H_∞ controller for the NRC bell 205 experimental fly-by-wire helicopter. In Proceedings of the AIAA Guidance, Navigation, and Control Conference and Exhibit, Boston, Massachusetts, USA, 1998, AIAA Paper 98–4300, Proceedings published on CD-ROM.
9 **La Civita, M., Papageorgiou, G., Messner, W. C.,** and **Kanade, T.** Design and flight testing of an H_∞ controller for a robotic helicopter. *J. Guid. Control Dyn.*, 2006, **29**(2), 485–494.
10 **Anonymous.** *Flying qualities of piloted aircraft, MIL-HDBK-1797*, 1997 (Department of Defense, USA).
11 **Francis, B. A.** *A course in H_∞ control theory*. Lecture Notes in Control and Information Sciences, Vol. 88, 1987 (Springer-Verlag, Berlin).
12 **Gu, D. W., Petkov, P. Hr.,** and **Konstantinov, M. M.** Robust control design with MATLAB®. In *Advanced textbooks in control and signal processing* (Eds M. J. Grimble, M. A. Johnson), 2005, p. 389 (Springer, London).
13 **Cervera, J.** and **Baños, A.** Nonlinear nonconvex optimization by evolutionary algorithms applied to robust control. *Math. Probl. Eng.*, 2009, **2009**, 1–22.
14 **Menon, P. P., Kim, J., Bates, D. G.,** and **Postlethwaite, I.** Clearance of nonlinear flight control laws using hybrid evolutionary optimization. *IEEE Trans. Evol. Comp.*, 2006, **10**(6), 689–699.
15 **Menon, P. P., Bates, D. G.,** and **Postlethwaite, I.** Deterministic versus evolutionary optimisation methods for nonlinear robustness analysis of flight control laws. In Proceedings of the 2007 IEEE Congress on *Evolutionary computation*, Singapore, 2007, Proceedings published on CD-ROM.
16 **Bourmistrova, A.** and **Khantsis, S.** Control system design optimisation via genetic programming. In Proceedings of the 2007 IEEE Congress on *Evolutionary computation*, Singapore, 2007, Proceedings published on CD-ROM.
17 **Droste, C. S.** *The general dynamics case study on the F16 fly-by-wire flight control system*, 1985 (AIAA Professional Series, New York).
18 **Minisci, E. A., Avanzini, G., D'Angelo, S.,** and **Dutto, M.** Multi–objective design of robust flight control systems. In Proceedings of ICNPAA 2008 (Mathematical Problems in Engineering, Aerospace and Sciences), Genova, Italy, 2008, Proceedings published on CD-ROM.
19 **Etkin, B.** *Dynamics of atmospheric flight*, 1972 (J. Wiley and Sons, New York).
20 **Larrañaga, P.** and **Lozano, J. A.** (Eds) *Estimation of distribution algorithms. a new tool for evolutionary computation*, 2002 (Kluwer Academic Publishers, Dordrecht).
21 **Mitchell, M.** *An introduction to genetic algorithms*, 1998 (The MIT Press, Boston).
22 **Khan, N., Golberg, D. E.,** and **Pelikan, M.** Multi-objective Bayesian optimisation algorithm, Technical Report IlliGAL 2002009, University of Illinois at Urbana-Champain - IlliGAL, USA, 2002.
23 **Costa, M.** and **Minisci, E.** MOPED: a multi-objective Parzen-based estimation of distribution algorithm. In Proceedings of EMO 2003, 2nd International Conference on *Evolutionary multi–criterion optimization*, Faro, Portugal, 2003, pp. 282–294.
24 **Avanzini, G., Biamonti, D.,** and **Minisci, E. A.** Minimum-fuel/minimum-time maneuvers of formation flying satellites. *Adv. Astronaut. Sci.*, 2003, **116**(III), 2403–2422.

APPENDIX

Notations

$\boldsymbol{A}$	state matrix
$\boldsymbol{B}$	control matrix
$\bar{c}$	mean aerodynamic chord
$\boldsymbol{C}$	output matrix
C_m	aerodynamic pitch moment coefficient
C_X, C_Z	aerodynamic force coefficients
$\boldsymbol{d}$	noise on output
g	gravity acceleration
h	altitude
$\boldsymbol{I}$	identity matrix
I_y	pitch moment of inertia
K_α, K_q, K_I	longitudinal SCAS gains
K_V, K_γ	autopilot gains
m	aircraft mass
M	Mach number
M_x	$= (1/I_y)\partial M/\partial x$, pitch moment stability/ control derivative
$\boldsymbol{n}$	sensor noise

$\boldsymbol{P}$	plant
q	pitch angular velocity
Q	$= 0.5\rho V^2$, dynamic pressure
$\boldsymbol{r}$	reference signal
s	Laplace variable
S	wing surface
$\boldsymbol{S}$, $\boldsymbol{T}$	sensitivity and complementary sensitivity functions
T	thrust
u, w	body-frame velocity components
$\boldsymbol{u}$	control vector
V	airspeed
$\boldsymbol{W}_i$	ith weight matrix
$\boldsymbol{x}$	state vector
X_x	$= (1/m)\partial X/\partial x$, longitudinal force stability/control derivative
$\boldsymbol{y}$	output vector
Z_x	$= (1/m)\partial Z/\partial x$, normal force stability/control derivative
α	angle of attack
γ	flight-path angle
δ_E	elevator deflection
δ_T	throttle setting
θ	pitch angle
ρ	air density
$\bar{\sigma}$	maximum singular value
τ	time constant

Subscripts

0	at trim, nominal
com	commanded
des	desired
F	filtered
max	maximum